Article

Cu₂O Homojunction Solar Cells: Efficiency Enhancement with a High Short Circuit Current

S. A. A. B. Thejasiri [1], K. M. D. C. Jayathilaka [1], F. S. B. Kafi [1], L. S. R. Kumara [2], O. Seo [2], S. Yasuno [2], O. Sakata [2], W. Siripala [1] and R. P. Wijesundera [1,*]

[1] Department of Physics and Electronics, University of Kelaniya, Kelaniya 11600, Sri Lanka; thejasiri94@gmail.com (S.A.A.B.T.); charithkmd@kln.ac.lk (K.M.D.C.J.); kafi@kln.ac.lk (F.S.B.K.); wps@kln.ac.lk (W.S.)

[2] Center for Synchrotron Radiation Research, Japan Synchrotron Radiation Research Institute (JASRI), 1-1-1 Kouto, Sayo-cho, Sayo-gun 679-5198, Hyogo, Japan; rosantha@spring8.or.jp (L.S.R.K.); seo.okkyun@spring8.or.jp (O.S.); yasuno@spring8.or.jp (S.Y.); sakata.osami@spring8.or.jp (O.S.)

* Correspondence: palitha@kln.ac.lk; Tel.: +94-7144458568

Abstract: Cu₂O homojunction solar cells were fabricated using potentiostatic electrodeposition technique. n-Cu₂O thin films were grown in an acetate bath while p-Cu₂O thin films were grown in a lactate bath. In the growth of n-Cu₂O films, cupric acetate concentration, pH and temperature of the bath, deposition potential and duration (film thickness) and annealing temperature were investigated. In the growth of p-Cu₂O on n-Cu₂O, concentration of copper sulphate and lactic acid solutions, pH and temperature of the bath, deposition potential and duration were investigated. In addition, the procedure of sulfidation of p-Cu₂O film surface using $(NH_4)_2S$ vapor, before depositing Au front contact, was also optimized to enhance the photoactive performance. The structural, morphological and optoelectronic properties of the Cu₂O films were investigated using scanning electron microscopy (SEMs), high energy X-ray diffraction (HEXRD), hard X-ray photoelectron spectroscopy (HAXPES), spectral response and current–voltage (J-V) measurements. The best Cu₂O homojunction solar cell exhibited V_{oc} = 460 mV, J_{sc} = 12.99 mA·cm^{-2}, FF = 42% and η = 2.51%, under AM 1.5 illumination. Efficiency enhancement with the record high J_{sc} value for the Cu₂O homojunction solar cell has mainly been due to the optimization of pH of the n-Cu₂O deposition bath and lactic acid concentration of the p-Cu₂O deposition bath.

Keywords: electrodeposition; Cu₂O; homojunction; short circuit current density

1. Introduction

Freely available abundant sunlight can be easily converted into electricity via Photovoltaic (PV) devices, which is a viable solution for preventing an energy crisis [1]. However, commercially available PV devices are relatively expensive; therefore, the research community focuses its attention on developing solar cells with low-cost materials and processing techniques. Recently, there has been increased attention to ultralow cost cuprous oxide (Cu₂O) material for PV applications due to its direct band gap of 2 eV, high absorption coefficient, material abundance, non-toxicity, possibility of growth of both n- and p-type conductivities and availability of large-area, low-cost growth techniques [2–12]. The conductivity of the Cu₂O is determined by the presence of lattice defects of cubic crystal structure having a lattice constant of 4.27 Å [13]. Until 1986, Cu₂O was known as a p-type material due to the Cu vacancies created in the lattice structure [14–20]. Therefore, earlier Cu₂O-based PV devices were fabricated as Schottky junctions or heterojunctions with suitable materials [2,21–28]. In 1986, the possibility of growth of n-Cu₂O was first reported by the method of electrodeposition in a slightly acidic bath by Siripala et al. [29]. Since then, n-Cu₂O thin films have been successfully grown by the electrodeposition method to use in many PV applications [8,30–34]. Now, it has been established that the electrodeposition

of Cu$_2$O films in acidic baths is attributed to n-type photoconductivity, and attributed to p-type photoconductivity in basic baths [30,35]. Interestingly, it is very important to utilize n-type conductive Cu$_2$O in developing low-cost PV junction devices since the electron affinity of Cu$_2$O is low compared to many low-cost oxide semiconductor materials; therefore, there is a very good potential for developing good quality low-cost junction devices. Among many possible junctions that may be developed for device applications, Cu$_2$O homojunction will be of great interest because lattice continuity across the junction reduces defects created at the interface, thereby reducing the density of defect electronic states created at the junction. However, finding a suitable low-cost fabrication method to produce a clean p-n homojunction of Cu$_2$O will be a challenging task. As reported previously, Cu$_2$O homojunction could be created using the inexpensive electrodeposition technique, which has advantages such as low cost, scalability, low-temperature process, etc. [36–38]. Notably, it is extremely important to be aware of the possibility of the introduction of thin interfacial layers or other defects at the electrodeposited p-n homojunction due to the inherent nature of the chemical processes involved in the electrodeposition method. Thus, when developing Cu$_2$O homojunction PV devices using the electrodeposition technique, the dependence of the device performance on deposition parameters will be at a crucial stage. In this investigation, we have focused on this aspect when improving the efficiency of Cu$_2$O homojunction solar cells.

The theoretical efficiency limit for the Cu$_2$O homojunction is 20% [39], but the reported efficiencies of Cu$_2$O homojunction solar cells were very low compared to the theoretical limit of 20%. In general, band continuity across the homojunction can be expected because band edge positions of both n- and p-materials are the same. However, junction properties may depend on the growth conditions and adopted fabrication techniques. As mentioned before, there is a possibility of growing a very thin interfacial layer at the junction during the electrodeposition process, leading to a band mismatch. Therefore, among other possibilities, interfacial mismatching at the p-n junction may be responsible for the reported poor efficiencies of Cu$_2$O homojunction solar cells. Kafi et al. explored the interfacial properties of n-Cu$_2$O/p-Cu$_2$O homojunction and reported that the relative band edge positions of n-Cu$_2$O and p-Cu$_2$O can be shifted by changing the pH of the n-Cu$_2$O and p-Cu$_2$O deposition baths [40]. The study showed that it was able to enhance the efficiency of the device with higher short circuit current density by adjusting the pH value of the deposition baths. Recent developments of the Cu$_2$O homojunctions are shown in Table 1. Previously, Jayathilaka et al. reported the highest efficiency of 2.64% for the Cu$_2$O homojunction solar cell while pre- and post-annealing of homojunction and surface sulfidation of n-Cu$_2$O and p-Cu$_2$O films have been useful for the improvement of the efficiency of Cu$_2$O homojunction device [41].

Table 1. Reported photoactive performance of Cu$_2$O homojunction solar cells.

V$_{oc}$ (mV)	J$_{sc}$ (mA·cm^{-2})	FF %	η %	Reference
320	1.23	35	0.102	[42] (2009)
423	2.5	27	0.29	[36] (2010)
621	4.07	42	1.06	[37] (2012)
120	3.97	23	0.104	[43] (2012)
420	2.68	38	0.42	[44] (2015)
287	12.4	25	0.89	[45] (2016)
490	12.8	-	2.64	[46] (2020)
324	12.67	30.7	1.3	[47] (2020)

In addition, we have reported earlier that the development of a Cu$_2$O homojunction is possible by improving the interfacial properties of the n-Cu$_2$O and p-Cu$_2$O homojunction, as well [47] where reported device performance was V$_{oc}$ of 324 mV, J$_{sc}$ of 12.67 mA·cm^{-2}, FF of 30.7% and η = 1.3%, under AM 1.5 artificial illumination. Therefore, as mentioned previously, when adapting the electrodeposition technique for the fabrication of the ho-

mojunction of Cu_2O, it is extremely important to study the effects of all the deposition parameters on the performance of the Cu_2O homojunction device.

To improve the performance of the Cu_2O homojunction device, in this study, the junction was started with previously reported fabrication conditions [47], and all the fabrication conditions were carefully fine-tuned. This led to enhancing the device's efficiency with the improvement of open circuit voltage, fill factor and, especially, short circuit current density to the highest reported value of 12.99 mA·cm^{-2}.

2. Experimental

Ti/n-Cu_2O/p-Cu_2O/Au homojunction device fabrication was initiated using previously optimized conditions [39]. We used 2×1 cm^2 Titanium sheets as a substrate for device fabrication. Then, Ti sheets were cleaned with detergent, diluted HCl, distilled water, and finally ultrasonicated in distilled water. Electrodeposition of n-Cu_2O thin films was potentiostatically carried out on Ti sheets at -200 mV vs. Ag/AgCl for 60 min in a three-electrode electrochemical cell having 0.1 M sodium acetate and 0.01 M cupric acetate. The counter and the reference electrodes were platinum plates and Ag/AgCl, respectively. Before the film deposition, the pH of the bath was adjusted to 6.1 by adding diluted HCl. During the deposition, the bath was stirred at 50 rve·min^{-1} and the bath temperature was maintained at 55 °C. After the film deposition, electrodes were immediately washed in distilled water and dried in air. All the Cu_2O/Ti electrodes were annealed at 100 °C for 24 h. p-Cu_2O thin films on n-Cu_2O/Ti electrodes were potentiostatically electrodeposited at -450 mV vs. Ag/AgCl for 45 min in a three-electrode electrochemical cell containing 3 M lactic acid, 0.4 M cupric sulfate and 4 M NaOH. The counter and the reference electrodes were platinum plate and Ag/AgCl, respectively. pH of the p-Cu_2O deposition bath was adjusted to 13.0 by adding NaOH solution to the bath. The temperature of the electrolyte was maintained at 60 °C and baths were continuously stirred at 200 rev·min^{-1} using a magnetic stirrer. After the film deposition, electrodes were immediately washed in distilled water and dried in air. For the surface modification of p-Cu_2O thin films, they were sulfided by exposing them to ammonium sulfide gas by simply holding the face down above a beaker containing 20 vol% $(NH_4)_2S$ solution at room temperature for 8 s and then the films were immediately thoroughly rinsed with distilled water. Thin Au spots having an area of $\sim 2 \times 2$ mm^2 were deposited by sputtering at 20 mA for 240 s on the sulfided p-Cu_2O thin films to obtain the front contact with the device. Electrical contacts to the junctions were made via the connections to the Ti substrate and Au spots. All the chemicals used were reagent grade. Devices fabricated under the above conditions were used as the control samples to monitor the change in performance during the fine-tuning stages of the fabrication conditions.

Fabrication conditions were optimized monitoring the photoactive performance of the complete device by changing one fabrication condition at a time. First, the growth conditions of the n-Cu_2O layer on the Ti substrate were optimized. Different sets of devices were prepared by changing the previous deposition conditions of the cupric acetate concentration of the bath, sodium acetate concentration of the bath, pH of the bath, stirring speed of the bath, temperature of the bath, deposition potential, deposition duration and annealing of the samples. Then growth conditions of the p-Cu_2O layer on n-Cu_2O were studied. Again, different sets of devices were prepared by changing the above condition of lactic acid concentration of the bath, cupric sulfate concentration of the bath, pH of the bath, stirring speed of the bath, temperature of the bath, deposition potential, deposition duration, for depositing p-Cu_2O on n-Cu_2O. Further, the sulfidation process was optimized by changing the exposure durations of 20 vol% $(NH_4)_2S$ solution, and growth conditions of the Au front contact layer deposition were optimized by changing the sputtering conditions. In addition to the Au sputtering, the vacuum coating technique was also tried out to grow the Au front contact. Hence, in this investigation, almost all possible p-n junction fabrication steps were optimized to maximize the performance of the Cu_2O homojunction solar cell device. Deposition solutions were prepared with distilled water and used reagent-grade

chemicals. Surface morphology of n- and p-films was studied using scanning electron microscopy (SEM).

Structural, morphological and optoelectronic characterizations of the devices were investigated. Surface morphology of n- and p-films was studied using scanning electron microscopy (SEM) using a Hitachi (SU6600) scanning electron microscope, Ibaraki, Japan. HEXRD experiment was conducted using the BL04B2 beamline at SPring-8, Sayo, Japan. A Si (220) monochromator was used to acquire incident X-rays with a wavelength of 0.20095 Å (energy $\simeq$ 61.7 keV), and the intensity of the incident X-rays was controlled by a monitored 99.99% Ar gas-filled ionization chamber. To minimize X-ray scattering from air, samples were stored in a vacuum bell jar. Three CdTe detectors were used to collect the diffracted X-rays over a broad angular range. For the HEXRD analysis, the Cu_2O thin film was scraped out from the Ti substrate and inserted into a fused silica capillary with dimensions of 1 mm inner diameter, 0.2 mm wall thickness, and 70 mm length. Hard X-ray photoelectron spectroscopy measurements were performed at BL46XU at SPring-8. The incident X-ray beam with photon energy 7.94 keV was monochromated using a Si (111) double crystal and a Si (444) channel-cut monochromator. Photoelectron spectra were observed using a hemispherical electron energy analyzer (R-4000L1-10kV, Scienta Omicron AB, Uppsala, Sweden). The opening of the analyzer slit was a 5 mm rectangle, and the passing energy was set to 200 eV. The analyzer was perpendicular to the X-ray axis and parallel to the polarization vector. The X-rays were incident at an incident angle of 80°, and the emitted photoelectrons were detected at an emission angle of 10° concerning the surface normal. The base pressure in the main chamber was between 1×10^{-6} to 5×10^{-6} Pa. All samples were connected to the ground of the HAXPES system via the sample holder.

The dark and light current–voltage characteristics of the devices were measured by chopping the white light of 1.5 AM. Spectral response measurements of the devices were obtained using a phase-sensitive detection method to monitor the photocurrent signal produced by a chopped monochromatic light beam at a chopping frequency of 53 Hz. The experimental setup consisted of a lock-in amplifier (Stanford Research-SR 830 DSP, Stanford Research Systems, CA, USA), a potentiostat (Hukoto Denko HAB 151, Hukoto Denko, Japan), a monochromator (Sciencetech 9010, Photonic Solutions Ltd., Edinburgh, UK) and a chopper (Stanford-SR 540, Stanford Research Systems, CA, USA).

3. Results and Discussion

To check the sensitivity of the depositing parameters on the n-Cu_2O films deposition for the p-n homojunction, different sets of devices were fabricated by slightly changing the predetermined deposition parameters of cupric acetate concentration of the bath around 0.01 M, sodium acetate concentration of the bath around 0.1 M, temperature of the deposition bath around 55 °C, stirring speed of the bath around 50 rev·min^{-1} and deposition potential around −200 mV vs. Ag/AgCl, by keeping the deposition conditions of the p-layer and the other deposition parameters to be the same. We have not observed any significant deviation in the performance of the homojunction device from the previously reported conditions for the growth of the n-Cu_2O layer [47]. Therefore, in this study, we have maintained these conditions when depositing n-Cu_2O layers for the homojunction.

Next, a set of devices was prepared by changing only the pH value of the deposition bath of n-Cu_2O films from 5.7 to 6.2, adding HCl to adjust the pH (the pH of the natural bath was 6.5). The photoactive properties of the resulting devices are shown in Table 2. Results revealed that the best pH for the n-Cu_2O film deposition bath when fabricating the p-n homojunction was 5.8. Further, Table 2 illustrates that the performance of the homojunction device is extremely sensitive to the pH of the deposition bath. This observation is very significant in developing Cu_2O homojunction devices. It has been reported previously that the relative band edge position of the n-Cu_2O can be shifted by adjusting the pH value of the n-Cu_2O deposition bath [40]. Therefore, the reason for the device fabricated with n-Cu_2O films deposited at the bath pH of 5.8 resulting in better performance, may be due to the better alignment of the band edge positions between n-Cu_2O and p-Cu_2O

layers of the p-n homojunction. Figure 1 shows the SEMs of the n-Cu_2O films deposited at (a) pH of 6.1 and (b) pH of 5.8. It has been previously reported that film morphology at the p-n junction could also determine the photovoltaic properties of the homojunction [36]. However, SEM images shown in Figure 1 do not suggest such a contrast in morphology; therefore, the observed remarkable increase in V_{oc} and I_{sc} values may not be due to the change in morphology alone. According to previous observations [40,48], the sensitivity of the pH to the relative flat band potential (or relative band edge position) of both p- and n-Cu_2O films in contact with electrolytes or metals will be the reason for the possibility of better alignment of the band edges at the junction.

Table 2. V_{oc} and J_{sc} values of devices grown under different n-Cu_2O bath pH values.

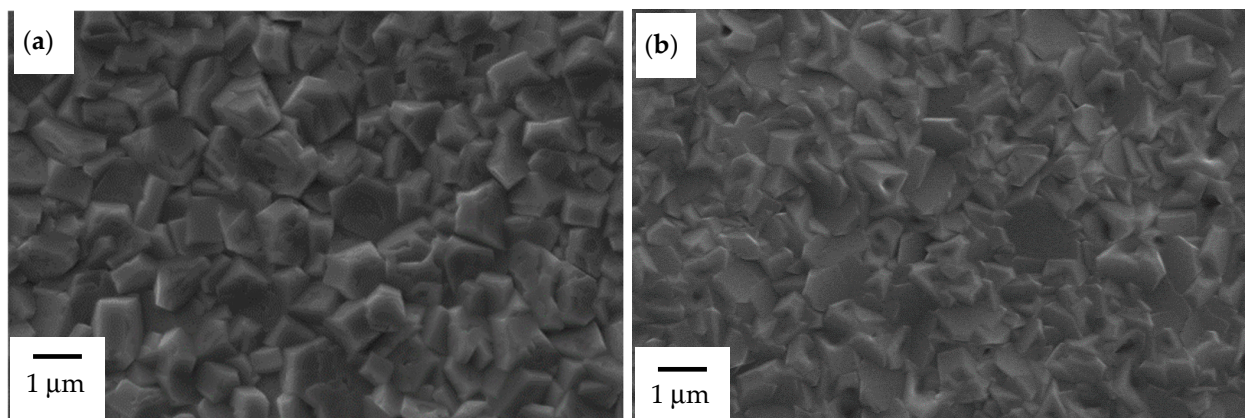| pH	5.7	5.8	5.9	6.0	6.1
V_{oc} (mV)	350	410	375	362	311
J_{sc} (mA·cm^{-2})	6.9	12.1	10.1	5.8	4.9

Figure 1. SEM images of n-Cu_2O films deposited in baths of (**a**) pH of 6.1 and (**b**) pH of 5.8.

In optimization of p-Cu_2O growth conditions when depositing p-Cu_2O on n-Cu_2O, different sets of devices were fabricated by slight change in the cupric sulfate concentration around 0.4 M, pH of the bath, temperature of the bath around 60 °C, stirring speed of the bath around 200 rev·min^{-1} and deposition potential around −450 mV vs. Ag/AgCl. The photoactive performance of the device revealed that the best cupric sulfate concentration, temperature of the deposition bath, stirring speed of the bath and deposition potential were 0.4 M, 60 °C, 200 rev·min^{-1} and −450 mV vs. Ag/AgCl, respectively, for the growth of p-Cu_2O, as reported earlier [47]. The dependency of the photoactive properties of the device on the lactic acid concentration of the bath is shown in Table 3. As shown in Table 3, the lactic acid concentration of the bath makes a huge impact on the photoactive performance of the device. The complexing agent lactic acid of the p-Cu_2O deposition bath determines the kinetics of Cu ions controlling the growth of the material [36].

Table 3. Lactate concentrations on p-Cu_2O deposition baths produced V_{oc} and J_{sc} values.

Lactic Acid Volume	Lactate Concentration	V_{oc} (mV)	J_{sc} (mA·cm^{-2})
20	2.28	406	4.35
22	2.51	445	12.88
24	2.74	421	7.68
26	2.97	399	6.05
28	3.19	340	8.30

The best lactic acid concentration of the bath to fabricate p-n homojunction is 2.51 M. The observed remarkable increase in the short circuit current and open circuit voltage will

be a very significant finding useful in developing the Cu_2O homojunction devices. This photoactive enhancement of the device with a lactic acid concentration of the bath has been further studied with the surface morphology of the p-Cu_2O films. Figure 2 shows the SEMs of the p-Cu_2O films deposited on n-Cu_2O films in a bath of (a) lactic acid concentration of 3 M and (b) lactic acid concentration of 2.51 M. A significant difference in the morphology of the films is evident in SEM images. The obvious difference between the two homojunction cells that can lead to the observed performance difference appears to be the large grain size in the film deposited with a lactic acid concentration of 2.51 M.
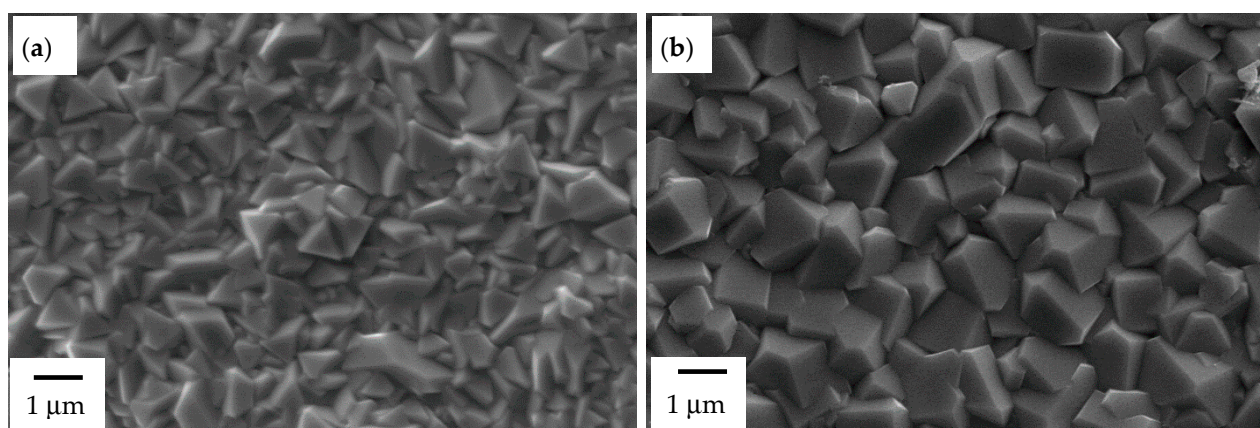

Figure 2. SEM of p-Cu_2O films deposited in a bath containing (**a**) lactic acid concentration of 3.00 M and (**b**) lactic acid concentration of 2.51 M.

The surface modification of p-Cu_2O thin films by exposing them to ammonium sulfide is a crucial step in the fabrication of Cu_2O homojunction devices. Therefore, sulfidation conditions were carefully re-examined. Table 4 shows the photoactive performance of the devices with different $(NH_4)_2S$ exposure durations. As observed, the best photoactivity was exhibited with the exposure of $(NH_4)_2S$ vapor for a duration of 8 s. To study the dependence of growth conditions of the front contacts, thin Au spots on the sulfided p-Cu_2O thin films were grown by changing the sputtering current and the duration. The photoactive performance of the devices revealed that the best sputtering conditions were 20 mA for 120 s.

Table 4. V_{oc} and J_{sc} values of devices with different exposure durations of $(NH_4)_2S$ vapor on p-Cu_2O film surfaces.

Time (s)	5	6	7	8	9	10
V_{oc} (mV)	372	384	396	445	321	292
J_{sc} (mA·cm^{-2})	2.4	2.5	6.4	12.8	11.3	10.6

Photoactive enhancement of the homojunction annealing in air was studied and Table 5 shows the photoactive performance of the device annealed at different temperatures for 30 min in air. Results revealed that the best annealing condition was 175 °C for 30 min.

Table 5. V_{oc} and J_{sc} of the samples were annealed for 30 min under different temperatures.

Annealed Temperature (°C)	V_{oc} (mV)	J_{sc} (mA·cm^{-2})
None	330	6.07
125	351	6.21
150	375	12.64
175	445	12.60
200	438	5.83

To maximize the generation and collection of photocarriers at the homojunction, it is very important to optimize the film thicknesses of the n- and p-type layers. For this, to estimate the film thicknesses of the layers, the total charge passed during the electrodeposition was measured. Two sets of devices were fabricated by changing the n-Cu_2O and p-Cu_2O deposition durations separately. Tables 6 and 7 show the photoactive performances of the devices with different n-Cu_2O and p-Cu_2O deposition durations (different film thicknesses). Results revealed that optimum n-Cu_2O and p-Cu_2O film thicknesses were 1.45 µm and 0.80 µm, respectively.

Table 6. V_{oc} and J_{sc} values of devices made with different n-Cu_2O layer thicknesses.

Time (minutes)	Charge (C)	Thickness (µm)	V_{oc} (mV)	J_{sc} (mA·cm^{-2})
20	1.297	1.07	406	9.72
30	1.764	1.45	447	12.90
40	2.187	1.80	414	12.04
50	2.576	2.12	300	5.95
60	2.936	2.42	272	5.08

Table 7. J_{sc} and V_{oc} values of the devices with different p-Cu_2O layer thicknesses.

Time (minutes)	Charge (C)	Thickness (µm)	V_{oc} (mV)	J_{sc} (mA·cm^{-2})
30	0.739	0.609	290	3.58
35	0.846	0.697	305	4.05
40	0.971	0.800	460	12.99
45	1.053	0.868	447	9.89
50	1.147	0.945	409	6.68

Structural information of n-Cu_2O and p-Cu_2O were studied using HEXRD measurements. Figure 3 shows the HEXRD spectra of electrodeposited n-Cu_2O and p-Cu_2O in acetate and lactate baths deposited using the optimum growth conditions stated above. The HEXRD spectra of n-Cu_2O and p-Cu_2O show analogous orientations with nine peaks corresponding to the reflections from (110), (111), (200), (220), (310), (311), (222), (321) and (400) atomic planes of Cu_2O. Additionally, HEXRD reveals a faint peak at 6.64° attributed to the (211) reflection of CuO indicating that the surface of Cu_2O interacts with air leading to the formation of CuO. Furthermore, structural information can be extracted from HEXRD by converting polarization, absorption and background-corrected data into total structure factor, $S(Q)$ and radial distribution functions (RDF) using Fourier transform $S(Q)$ [49]. Figure 3c displays the RDF spectra of n Cu_2O (black) and p Cu_2O (red), showing similar RDF distributions with identical peak positions for both types. The first and second peaks in Figure 3c indicate that the Cu-O and Cu-Cu correlations are 1.87 Å and 3.04 Å, respectively. The correlation agrees with the Cu-O (1.849 Å) and Cu-Cu (3.012 Å) correlations found in standard Cu_2O powder [50].

The HAXPES spectra of *n*-Cu_2O prepared at pH 5.8 (black) in Figure 4a show that the binding energies of the Cu $2p_{1/2}$ and Cu $2p_{3/2}$ are 953.1 and 933.1 eV, respectively, which are consistent with the binding energy values for Cu(I) reported in the literature as 952.5 and 932.18 eV. A weak spike was observed at 947.3 indicating the slight oxidation of Cu(I) to Cu(II) possibly present on the surface forming CuO [51]. It could be due to the surface oxidation of Cu_2O while sample handling in air.

The XPS spectra of the *p*-Cu_2O prepared at pH 13 (red line) in Figure 4a have slightly shifted to the left, showing peaks for Cu $2p_{1/2}$ and Cu $2p_{3/2}$ at 951.8 and 931.8 eV binding energies, respectively, which are also consistent with the Cu (I) oxidation state.
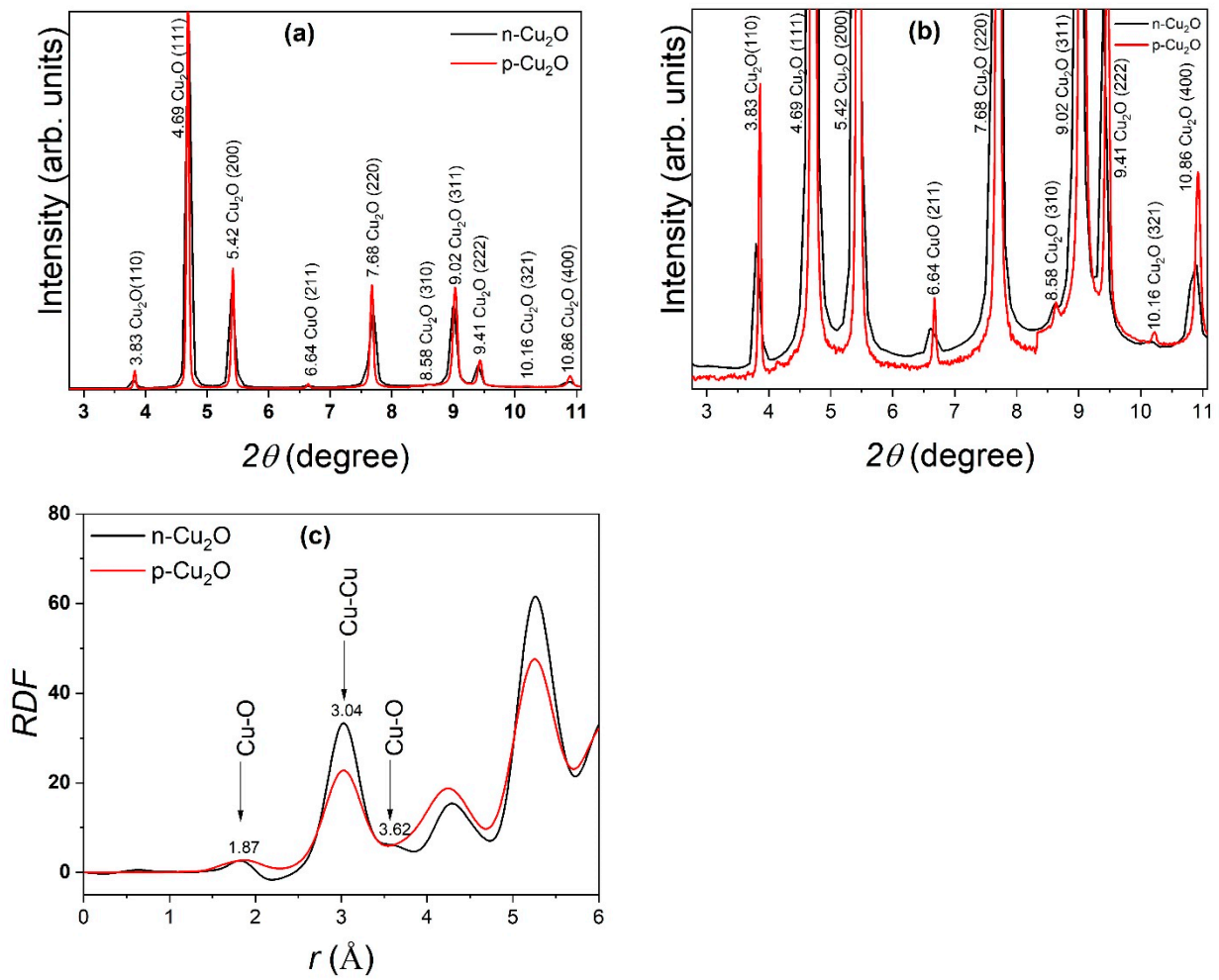
Figure 3. (**a**) HEXRD spectra of Cu$_2$O thin films; n-Cu$_2$O prepared at pH 5.8 (black), p-Cu$_2$O prepared at pH 13 (red). (**b**) Enlarged spectra. (**c**) Radial distribution functions of n Cu$_2$O prepared at pH 5.8 (black), p-Cu$_2$O prepared at pH 13 (red).
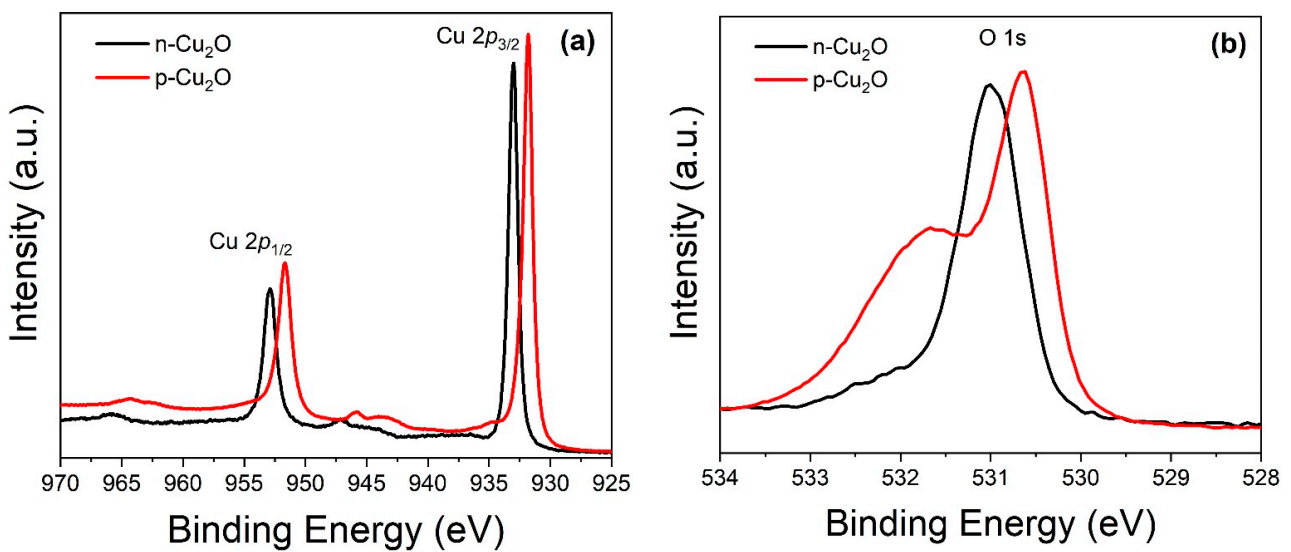

Figure 4. (**a**) HAXPES spectra of Cu 2p region of Cu$_2$O thin films: n Cu$_2$O prepared at pH 5.8 (black), p Cu$_2$O prepared at pH 13 (red). (**b**) HAXPES spectra of O 1s region of Cu$_2$O thin films: n Cu$_2$O prepared at pH 5.8 (black), p Cu$_2$O prepared at pH 13 (red).

As shown in Figure 4b, the O1s core-level spectrum is broad, with a peak at 531.0 eV for *n*-Cu_2O and a peak at 530.7 eV for *p*-Cu_2O, which are consistent with the values in the literature for Cu_2O. Additionally, the O1s spectrum of *p*-Cu_2O shows a broad shoulder peak at 531.7 eV. This is typically indicative of oxygen species that are different from the lattice oxygen of the Cu_2O structure. Adsorbed hydroxyl groups/water molecules on the surface of Cu_2O can give rise to a broad peak in the O 1s spectrum around 531.5–532.5 eV [52]. These hydroxyl groups could be a result of exposure to ambient moisture.

A slight increase in the binding energies of *n*-type Cu_2O compared to *p*-type Cu_2O could be due to the increased electron density in the conduction band of *n*-type Cu_2O. These electrons are in a relatively stable and low-energy state, causing a higher binding energy.

The HAXPES analysis is consistent with the XRD results, further confirming that Cu_2O has been successfully synthesized.

Light-generated J-V characteristics of the Cu_2O homojunctions solar cells are given in Figure 5 for the control sample and the cell fabricated with fine-tuning the conditions. It is important to notice that when comparing with the V_{oc} of 324 mV, J_{sc} of 12.67 mA·cm^{-2}, FF of 30.7% and η = 1.3% of the control sample, the performance of the fine-tuned Cu_2O homojunction solar cell has significantly increased to V_{oc} of 460 mV, J_{sc} of 12.99 mA·cm^{-2}, FF of 42% and η = 2.51%. Still, it is evident in Figure 5, J-V characteristics should be further improved because the poor fill factor contributes primarily to the low-efficiency value. High series resistance and low shunt resistance have contributed to this result and need to be improved. Although the efficiency of the Cu_2O homojunction solar cell is limited to 2.51%, the remarkably high J_{sc} is encouraging. This short circuit current density, to our knowledge, is the highest reported value for an electrodeposited Cu_2O homojunction device. This device may be readily applicable in large-area optical device applications where short circuit current density will be a primary objective, such as in optical sensors.
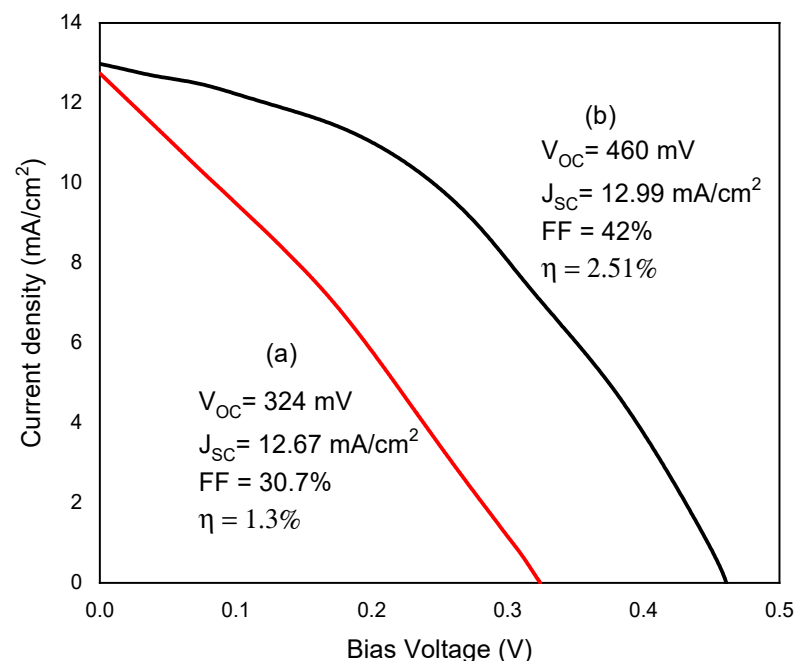

Figure 5. Photocurrent Density—Voltage characteristics of (a) before (red line) and (b) after optimization of the fabrication (black line).

Spectral responses of the control sample and the best device are shown in Figure 6. The spectral response curves of both devices were almost the same except for a slight increase in the photocurrent in the short wavelength region of 500 nm to 550 nm of the device fabricated with fine-tuning.
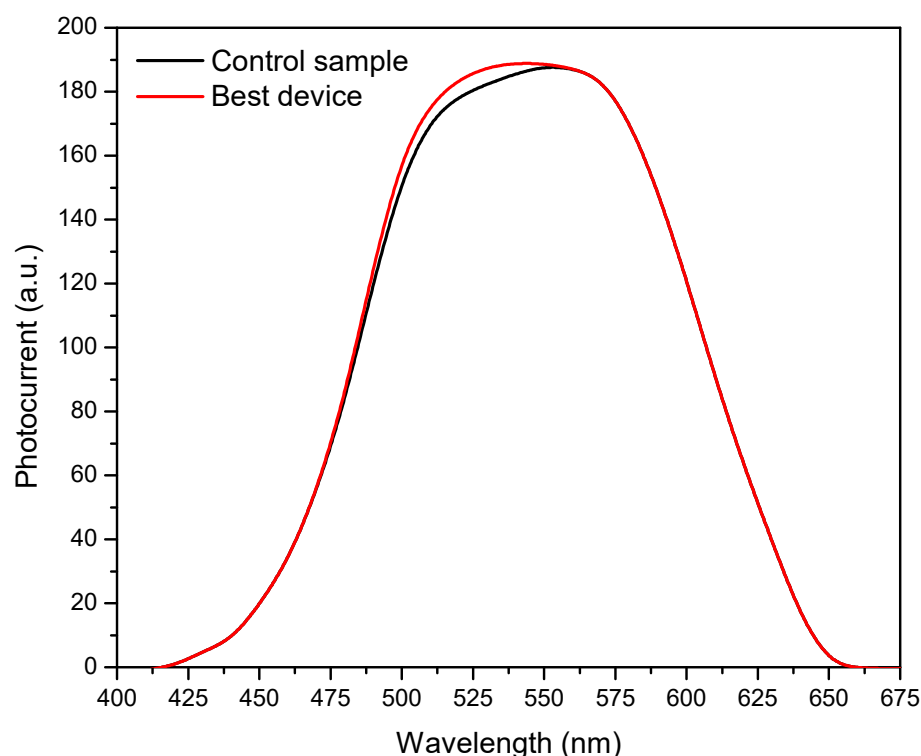
Figure 6. Spectral responses of the control sample and the best-performing device.

4. Conclusions

In this study, the possibility of improving the efficiency of the Cu_2O homojunction solar cell was investigated by fine-tuning the Cu_2O homojunction fabrication conditions. We have demonstrated the possibility of enhancing the efficiency of the Cu_2O homojunction solar cell with a high short circuit current density by fine-tuning the n-Cu_2O growth parameters in the acetate bath and p-Cu_2O growth parameters in the lactate bath. The best photoresponse was produced by a Cu_2O homojunction solar cell when 1.45 μm thin n-Cu_2O film was grown using a bath containing 0.1 M sodium acetate and 0.01 M cupric acetate solution at the pH of 5.8 and 0.8 μm thin p-Cu_2O was grown using a bath containing 2.51 M lactic acid, 0.4 M cupric sulfate and 4 M NaOH solution at the pH of 13. As revealed by the photocurrent density voltage measurements, the device exhibits the highest reported short circuit current density for an electrodeposited Cu_2O homojunction solar cell. The homojunction solar cell structure of Ti/n-Cu_2O/p-Cu_2O/Au produced V_{oc} of 460 mV, J_{sc} of 12.99 mA·cm^{-2}, FF of 42% and η = 2.51% under AM 1.5 artificial illumination. Although the overall power conversion efficiency of the device is on the lower side, as a large area optical device, this device has potential applications. Major limitations of the device that have been able to produce in this study are the low fill factor and V_{oc} values.

Author Contributions: R.P.W., S.A.A.B.T., K.M.D.C.J., F.S.B.K. and W.S. designed the research. S.A.A.B.T. and K.M.D.C.J. prepared the samples., S.A.A.B.T., K.M.D.C.J., L.S.R.K., O.S. (O. Seo) and S.Y., performed experiments. R.P.W., W.S., S.A.A.B.T., K.M.D.C.J., F.S.B.K., L.S.R.K., O.S. (O. Seo), S.Y. and O.S. (O. Sakata) analyzed the data. R.P.W., K.M.D.C.J. and L.S.R.K. wrote the manuscript. All authors have read and agreed to the published version of the manuscript.

Institutional Review Board Statement: Not applicable.

Informed Consent Statement: Not applicable.

References

1. Chapin, D.M.; Fuller, C.S.; Pearson, G.L. A New Silicon p-n Junction Photocell for Converting Solar Radiation into Electrical Power. *J. Appl. Phys.* **1954**, *25*, 676–677. [CrossRef]
2. Olsen, L.C.; Addis, F.W.; Miller, W. Experimental and theoretical studies of Cu_2O solar cells. *Sol. Cells* **1982**, *7*, 247–279. [CrossRef]
3. Rai, B.P. Cu_2O solar cells: A review. *Sol. Cells* **1988**, *25*, 265–272. [CrossRef]
4. Briskman, R.N. A study of electrodeposited cuprous oxide photovoltaic cells. *Sol. Energy Mater. Sol. Cells* **1992**, *27*, 361–368. [CrossRef]
5. Katayama, J.; Ito, K.; Matsuoka, M.; Tamaki, J. Performance of Cu_2O/ZnO solar cell prepared by two-step electrodeposition. *J. Appl. Electrochem.* **2004**, *34*, 687–692. [CrossRef]
6. Rakhshani, A.E. Preparation, characteristics and photovoltaic properties of cuprous oxide-a review. *Solid-State Electron.* **1988**, *29*, 7–17. [CrossRef]
7. Raebiger, H.; Lany, S.; Zunger, A. Origins of the p-type nature and cation deficiency in Cu_2O and related materials. *Phys. Rev. B* **2007**, *76*, 045209. [CrossRef]
8. Xiong, L.; Huang, S.; Yang, X.; Qiu, M.; Chen, Z.; Yu, Y. p-Type and n-type Cu_2O semiconductor thin films: Controllable preparation by simple solvothermal method and photoelectrochemical properties. *Electrochim. Acta* **2011**, *56*, 2735–2739. [CrossRef]
9. Güneri, E.; Aker, D.; Henry, J.; Billur, C.A.; Saatçi, B. Cu_2O thin films prepared by chemical bath deposition: An improved method. *Phase Transit.* **2022**, *95*, 679–690. [CrossRef]
10. Chen, C.; Xu, L.; Dong, J.K. Direct growth and shape control of Cu_2O film via one-step chemical bath deposition. *Thin Solid Film.* **2013**, *527*, 76–80. [CrossRef]
11. Laidoudi, S.; Bioud, A.Y.; Azizi, A.; Schmerber, G.; Bartringer, J.; Barre, S.; Dinia, A. Growth and characterization of electrode-posited Cu_2O thin films. *Semicond. Sci. Technol.* **2013**, *28*, 115005. [CrossRef]
12. Wu, L.; Tsui, L.; Swami, N.; Zangari, G. Photoelectrochemical Stability of Electrodeposited Cu_2O Films. *J. Phys. Chem. C* **2010**, *114*, 11551–11556. [CrossRef]
13. Ghijsen, J.; Tjeng, L.H.; van Elp, J.; Eskes, H.; Westerink, J.; Sawatzky, G.A. Electronic structure of Cu_2O and CuO. *Phys. Rev.* **1988**, *38*, 11322–11330. [CrossRef] [PubMed]
14. Pollack, G.P.; Trivich, D. Photoelectic properties of cuprous oxide. *J. Appl. Phys.* **1975**, *46*, 163–172. [CrossRef]
15. Guy, A.C. *Introduction to Material Science*; Mcgraw-Hill: Tokyo, Japan, 1972.
16. Kaufman, R.G.; Hawkins, R.T. Defect luminescence of thin films of Cu_2O on copper. *J. Electrochem. Soc.* **1984**, *131*, 385–388. [CrossRef]
17. Wright, A.F.; Nelson, J.S. Theory of the copper vacancy in cuprous oxide. *J. Appl. Phys.* **2002**, *92*, 5849–5851. [CrossRef]
18. Harukawa, N.; Murakami, S.; Tamon, S.; Ijuin, S.; Ohmori, A.; Abe, K.; Shigenari, T. Temperature dependence of luminescence lifetime in Cu_2O. *J. Lumin.* **2000**, *87–89*, 1231–1233. [CrossRef]
19. Paul, G.K.; Nawa, Y.; Sato, H.; Sakurai, T.; Akimoto, K. Defects in Cu_2O studied by deep level transient spectroscopy. *Appl. Phys. Lett.* **2006**, *88*, 141901. [CrossRef]
20. Rajshekar, K.; Kannadassan, D. p-Type Cu_2O Thin Film Transistors for Active Matrix Displays: Physical Modeling and Numerical Simulation. *IEEE Access* **2021**, *9*, 158842–158851. [CrossRef]
21. Tanaka, H.; Shimakawa, T.; Miyata, T.; Sato, H.; Minami, T. Electrical and optical properties of TCO–Cu_2O heterojunction devices. *Thin Solid Films* **2004**, *469*, 80–85. [CrossRef]
22. Sears, W.M.; Fortin, E.; Webb, J.B. Indiumtinoxide/Cu_2O photovoltaic cells. *Thin Solid Films* **1983**, *103*, 303–309. [CrossRef]
23. Hames, Y.; San, S.E. CdO/Cu_2O solar cells by chemical deposition. *Sol. Energy* **2004**, *77*, 291–294. [CrossRef]
24. Papadimitriou, L.; Economou, N.A.; Trivich, D. Heterojunction solar cells on cuprous oxide. *Sol. Cell* **1981**, *3*, 73–80. [CrossRef]
25. Herion, J.; Niekisch, E.A.; Scharl, G. Investigation of metal oxide/cuprous oxide heterojunction solar cells. *Sol. Energy Mater.* **1980**, *4*, 101–112. [CrossRef]
26. Minami, T.; Nishi, Y.; Miyata, T. High-Efficiency Cu_2O-Based Heterojunction Solar Cells Fabricated Using a Ga_2O_3 Thin Film as N-Type Layer. *Appl. Phys. Express* **2013**, *6*, 044101. [CrossRef]
27. Minami, T.; Tanaka, H.; Shimakawa, T.; Miyata, T.; Sato, H. High-Efficiency Oxide Heterojunction Solar Cells Using Cu_2O Sheets. *Jpn. J. Appl. Phys.* **2004**, *43*, L917. [CrossRef]
28. Mittiga, A.; Salza, E.; Sarto, F.; Tucci, M.; Vasanthi, R. Heterojunction solar cell with 2% efficiency based on a Cu_2O substrate. *Appl. Phys. Lett.* **2006**, *88*, 163502. [CrossRef]
29. Siripala, W.; Jayakody, J.R.P. Observation of n-type photoconductivity in electrodeposited copper oxide film electrodes in a photoelectrochemical cell. *Sol. Energy Mater.* **1986**, *14*, 23–27. [CrossRef]

30. Wang, L.; Tao, M. Fabrication and characterization of p–n homojunctionsin cuprous oxide by electrochemical deposition. *Electrochem. Solid-State Lett.* **2007**, *10*, H248–H250. [CrossRef]

31. Siegfried, M.J.; Choi, K.S. Elucidation of an overpotential-limited branching phenomenon observed during the electrocrystallization of cuprous oxide. *Angew. Chem. Int. Ed.* **2008**, *47*, 368–372. [CrossRef]

32. McShane, C.M.; Choi, K.S. Photocurrent enhancement of n-type Cu$_2$O electrodes achieved by controlling dendritic branching growth. *J. Am. Chem. Soc.* **2009**, *131*, 2561–2569. [CrossRef]

33. Musa, A.O.; Akomolafe, T.; Carter, M.J. Production of cuprous oxide, a solar cell material, by thermal oxidation and a study of its physical and electrical properties. *Sol. Energy Mater. Sol. Cells* **1998**, *51*, 305–316. [CrossRef]

34. Jiang, T.; Xie, T.; Yang, W.; Fan, H.; Wang, D. Photoinduced charge transfer process in p-Cu$_2$O/n–Cu$_2$O homojunction film and its photoelectric gas-sensing properties. *J. Colloid Interface Sci.* **2013**, *405*, 242–248. [CrossRef] [PubMed]

35. Wang, W.; Wu, D.; Zhang, Q.; Wang, L.; Tao, M. pH-dependence of conduction type in cuprous oxide synthesized from solution. *J. Appl. Phys.* **2010**, *107*, 123717–123718. [CrossRef]

36. McShane, C.M.; Siripala, W.; Choi, K.S. Effect of junction morphology on the performance of polycrystalline Cu$_2$O homojunction solar cells. *J. Phys. Chem. Lett.* **2010**, *1*, 2666–2670. [CrossRef]

37. McShane, C.M.; Choi, K.S. Junction studies on electrochemically fabricated p–n Cu$_2$O homojunction solar cells for efficiency enhancement. *Phys. Chem. Chem. Phys.* **2012**, *14*, 6112–6118. [CrossRef]

38. Yu, L.; Xiong, L.; Yu, Y. Cu$_2$O Homojunction Solar Cells: F-Doped N-type Thin Film and Highly Improved Efficiency. *Phys. Chem. C* **2015**, *119*, 22803–22811. [CrossRef]

39. Shockley, W.; Queisser, H.J. Detailed balance limit of efficiency of pn junction solar cells. *J. Appl. Phys.* **1961**, *32*, 510–519. [CrossRef]

40. Kafi, F.S.B.; Jayathileka, K.M.D.C.; Wijesundera, R.P.; Siripala, W. Effect of Bath pH on Interfacial Properties of Electrodeposited n-Cu$_2$O Films. *Phys. Status Solidi B* **2018**, *255*, 1700541. [CrossRef]

41. Jayathilaka, K.M.D.C.; Kapaklis, V.; Siripala, W.; Jayanetti, J.K.D.S. Ammonium sulfide surface treatment of electrodeposited p-type cuprous oxide thin films. *Electron. Mater.Lett.* **2014**, *10*, 379–382. [CrossRef]

42. Han, K.; Tao, M. Electrochemically deposited p-n homojunction cuprous oxide. *Sol. Energy Mater. Sol. Cells* **2009**, *93*, 153–157. [CrossRef]

43. Wei, H.M.; Gong, H.B.; Chen, L.; Zi, M.; Cao, B.Q. Photovoltaic Efficiency Enhancement of Cu$_2$O Solar Cells Achieved by Controlling Homojunction Orientation and Surface Microstructure. *J. Phys. Chem. C* **2012**, *116*, 10510–10515. [CrossRef]

44. Hsu, Y.K.; Wu, J.R.; Chen, M.H.; Lin, Y.G. Fabrication of homojunction Cu$_2$O solar cells by electrochemical deposition. *Appl. Surf. Sci.* **2015**, *354*, 8–13. [CrossRef]

45. Wijesundera, R.P.; Gunawardhana, L.K.A.D.D.S.; Siripala, W. Electrodeposited Cu$_2$O homojunction solar cells: Fabrication of a cell of high short circuit photocurrent. *Sol. Energy Mater. Sol. Cells* **2009**, *157*, 881–886. [CrossRef]

46. Jayathilaka, C.; Kumara, L.S.R.; Ohara, K.; Song, C.; Kohara, S.; Sakata, O.; Siripala, W.; Jayanetti, S. Enhancement of Solar Cell Performance of Electrodeposited Ti/n-Cu$_2$O/p-Cu$_2$O/Au Homojunction Solar Cells by Interface and Surface Modification. *Crystals* **2020**, *10*, 609. [CrossRef]

47. Kafi, F.S.B.; Wijesundera, R.P.; Siripala, W. Low-cost Electrodeposited Cuprous Oxide Homojuncton Solar Cell. In Proceedings of the SLTw Webinar 2020 on Applied Research for Sustainable Development, Online, 24 November 2020; pp. 27–32.

48. Kafi, F.S.B.; Jayathileka, K.M.D.C.; Wijesundera, R.P.; Siripala, W. Dependence of interfacial properties of p-Cu$_2$O/electrolyte and p-Cu$_2$O/Au junctions on the electrodeposition bath pH of p-Cu$_2$O films. *Mater. Res. Express* **2018**, *5*, 086406. [CrossRef]

49. Kohara, S.; Itou, M.; Suzuya, K.; Inamura, Y.; Sakurai, Y.; Ohishi, Y.; Takata, M. Structural studies of disordered materials using high-energy x-ray diffraction from ambient to extreme conditions. *J. Phys. Condens. Matter* **2007**, *19*, 506101. [CrossRef]

50. Ruiz, E.; Alvarez, S.; Alemany, P.; Evarestov, R.A. Electronic structure and properties of Cu$_2$O. *Phys. Rev. B* **1997**, *56*, 7189–7196. [CrossRef]

51. Biesingera, M.C.; Laua, L.W.M.; Gerson, A.R.; Smart, R.S.C. Resolving surface chemical states in XPS analysis of first row transition metals, oxides and hydroxides: Sc, Ti, V, Cu and Zn. *Appl. Surf. Sci.* **2010**, *257*, 887–898. [CrossRef]

52. Biesinger, M.C.; Payne, B.P.; Grosvenor, A.P.; Lau, L.W.M.; Gerson, A.R.; Smart, R.S.C. Resolving surface chemical states in XPS analysis of first row transition metals, oxides and hydroxides: Cr, Mn, Fe, Co and Ni. *Appl. Surf. Sci.* **2011**, *257*, 2717–2730. [CrossRef]